



## PERFORMANCE ANALYSIS OF SEISMICALLY EXCITED STATUES IN FIXED-BASE AND BASE-ISOLATED CONDITIONS

Stefano SORACE<sup>1</sup> and Gloria TERENCE<sup>2</sup>

### ABSTRACT

A study concerning the evaluation of seismic response of statues exhibited in art museums, and a base-isolated floor strategy for their enhanced protection, are presented in this paper. Attention is particularly focused on statues made of small tensile strength materials, whose behaviour is simulated by a smeared-crack finite element approach. Seismic performance is assessed by referring to four levels specially postulated herein, and namely: 1) Rest conditions; 2) No rocking; 3) Damage control; and 4) Collapse prevention. The response is investigated via incremental dynamic analysis, by progressively increasing the amplitude of the ground motion histories adopted as inputs, and by relating output data to the limit conditions fixed for the above-mentioned performance levels. The assessment procedure is applied to a demonstrative case study, represented by a marble statue to be exhibited in the museum wing situated at the ground level of a medieval castle in Italy, according to an architectural hypothesis of partial rebuilding and reuse of the stronghold. The design solution for the base-isolated floor consists in a system of double-friction pendulum isolators. The finite element model constitutive laws and parameters, the dynamic analyses carried out in fixed-base and base-isolated floor conditions, and the practical implementation of the assumed performance assessment criteria are reported for the statue examined, along with a selection of technical details of the floor design.

### INTRODUCTION

Severe damage to art objects and museum contents is often induced by moderate to severe earthquakes, even when the buildings where they are exhibited are only slightly injured. This is a consequence of the peculiar dynamic behaviour of the artefacts, which can include sliding, tilting and rocking. These effects can cause the objects to lose equilibrium, and thus overturn and fall off. In view of this, the response of exhibits has been traditionally analysed within the context of the dynamics of rigid blocks (Caliò and Marletta 2003). This approach is still useful for a first-level evaluation of the safety conditions of any type of artworks, and represents an exhaustive assessment criterion for assets characterized by little deformability, among which caskets, reliquaries, show-cases, cabinets and other exhibition furniture and fittings. All overturning control-based methods allow evaluating the maximum seismic action for which this limit condition is not reached, and thus they implicitly focus on the basic performance level (PL) represented by Collapse prevention.

A second-level assessment analysis, which can be an option for rigid artworks, is strictly required for more deformable objects, including statues, busts, pots, amphorae and steles. Indeed, in these cases a careful evaluation of the damage effects induced by internal strain and stress states, also when the response is stable in terms of dynamic equilibrium, is as important as the verifications about

<sup>1</sup> Assoc. Prof., University of Udine, Udine, Italy, stefano.sorace@uniud.it

<sup>2</sup> Assist. Prof., University of Florence, Florence, Italy, terenzi@dicea.unifi.it

overturning. This is especially true when these artefacts are made of small tensile strength materials, such as marble, stone, terracotta and ceramics (representing most of museum contents), because cracks can arise in their most stressed zones even at low earthquake amplitudes. Hence, at least a second PL must be considered in the assessment process, concerning the Damage control of the object, for the preservation of its artistic value (Augusti and Ciampoli 1996).

A research study dedicated to the seismic assessment of art objects and the conception and implementation of a novel strategy for their enhanced protection is presented in this paper, where attention is particularly focused on statues made of small tensile strength materials. A more articulated set of performance levels is formulated for the assessment procedure, as compared to the above-mentioned criteria referred to the Damage control and Collapse prevention PLs only. Rocking and sliding effects are expressly taken into account, so as to evaluate their influence on seismic response, investigated via an incremental dynamic finite element analysis. A special base isolation strategy is then proposed as seismic protection solution, extended here to the entire bearing floor rather than to single statues, as currently applied in art museums situated in several earthquake-prone countries. The assessment procedure is demonstratively applied to a marble statue to be exhibited, along with other sculptures of similar dimensions, in the new museum wing of a medieval castle located in the town of Magnano in Riviera, Friuli-Venezia Giulia region, Italy. The behaviour of the statue is simulated by a smeared-crack finite element approach, which allows following carefully the evolution of crack-related damage. The isolation solution designed for the floor, that is, a system of identical double-friction pendulum (DFP) isolators, is described by including key technical details of installation. The performance of the statue in base-isolated floor conditions is finally examined, to evaluate the benefits resulting from the incorporation of the protective technology.

## **FORMULATION OF SEISMIC PERFORMANCE LEVELS**

When a statue is not firmly fixed to the floor or its pedestal, an exhaustive description of its dynamic behaviour must include the evaluation of possible rocking effects, because these can amplify internal stress and strain states, as well as cause local damage to the base section. In this respect, with a view to carefully following the evolution of seismic response from the lowest amplitudes of the input ground motions, the following two PLs are established: 1) Rest, and 2) No rocking. The first level corresponds to the transmission of purely compressive normal stresses from the base of the statue to the floor or the top of the pedestal, if applicable, which causes the object to respond identically for stationary and free contact mounts. Rest conditions terminate when the first decompression of a joint belonging to the base section is reached. Although not coinciding with the attainment of rocking, this configuration can already determine non negligible local amplifications of the response parameters, and thus it must be checked properly. The boundary of level 2) corresponds to the appearance of rocking, which is identified by repeated uplifts of a set of joints belonging to one or more sides of the base section. In order to quantitatively evaluate the attainment of this limit condition, a criterion concerning the number and amplitudes of uplifts must be proposed. Based on the results of finite element enquiries carried out on several sculptures, the minimum number of uplifts can be fixed at five, and their amplitude at around 0.5 mm. These values are proposed here as a reference, but they can be obviously calibrated case by case to adapt to the specific characteristics of any sculpture.

The set of PLs is completed by the two classical levels discussed in the Introduction, i.e. 3) Damage control, and 4) Collapse prevention. The upper limit of level 3) is assumed as coinciding with the appearance of visible cracks, for statues made of small tensile strength materials, or local plasticizations, for bronze and other metallic sculptures. These represent limit conditions for the safeguard of the artistic value of the asset too. Therefore, the performance level of Damage control can also be labelled as “Artistic value safety”. It can be noted that, although significant earthquake damage could in principle arise before the appearance of rocking, in which case level 3) would precede 2), several real case studies show that the most important damage generally follows the activation of rocking response conditions. A second observation specifically concerns statues made of small tensile strength materials, whose cracking-related damage evolution should be properly analysed by means of smeared-crack computational models, as observed above. However, approximate evaluations of crack spread and related damage can also be deduced from conventional linear elastic finite element

approaches, by comparing the maximum tensile stress values deriving from the analysis with the nominal tensile strength of the constituting material.

Similarly to the No rocking PL, a quantitative criterion is needed to help evaluate the attainment of the limit condition of the Damage control level too. This consists in establishing an upper threshold for crack spreading, which can be fixed in the opening of cracks at 5% of the total of Gauss points of the model. This information can be directly drawn from the results of the analysis, in a smeared-crack computation, or approximately estimated with a linear elastic model, by comparing the peak tensile stresses calculated in the Gauss points of the most stressed zones of the mesh with the assumed tensile strength, according to the observation above.

The limit conditions of performance level 4) are represented by the achievement of overturning-induced loss of stability or structural collapse. Normally, the former condition is not expressly highlighted in output by the finite element analysis, but it can be easily deduced from the time-history response, by comparing the seismically induced overturning moment with the available resisting moment due to gravity, both computed with respect to the instantaneous center of rotation. The condition of structural collapse is explicated by the divergence of the numerical solution, for smeared-crack models, whereas for elastic analyses the evaluation of tensile stress states carried out for the assessment of level 3) must be extended, so as to approximately locate the failure of the most stressed section(s) of the statue.

Levels 1) and 2) are not considered for elements in stationary contact with their support, for which the assessment enquiry is limited to the basic PLs of Damage control and Collapse prevention.

## CASE STUDY STATUE

The statue examined in this study, a view of which is shown in Figure 1, is a 17<sup>th</sup> century marble copy of a Hellenistic sculpture reproducing the Greek philosopher Socrates. The statue is constituted by a monolithic block including a thin parallelepiped pedestal, with square base section of 650 mm per side and height of 180 mm. The total height of the statue is about 1850 mm. Its aspect ratio is rather similar to the sculpture displayed on the left in Fig. 1, although with greater overall dimensions. On the other hand, due to the incorporation of the pedestal, global stability conditions are more favorable, and sensitivity to rocking is lower.

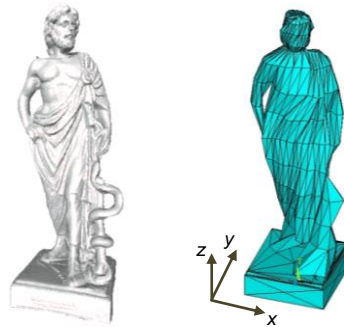


Figure 1. View of case study statue and relevant finite element model

The statue is made of greyish Carrara marble, with fine average grain size (below 1000  $\mu\text{m}$ ) and in good conservation state. As no characterization tests were carried out on the material, its mechanical properties were established by referring to the following typical ranges of variation suggested in literature (Scesi et al. 2006): uniaxial compressive strength  $f_c=40\text{--}70$  MPa; uniaxial tensile strength  $f_t=1.5\text{--}4$  MPa; Young modulus  $E=50,000\text{--}60,000$  MPa; specific weight  $\gamma=25\text{--}27$  kN/m<sup>3</sup>. In consideration of the ageing and creep-related strength decay occurring throughout the structural life of marbles and stones (Sorace 1996, 1998), the lowest values of the  $f_c$  and  $f_t$  ranges above, i.e.  $f_c=40$  MPa and  $f_t=1.5$  MPa, were assumed as basic choices in the analysis. However,  $f_t$ , whose value is the most critical parameter in smeared-crack computation, was raised to 3 MPa, in order to evaluate its influence on the performance of the statue, as discussed in section 4 below.

Concerning  $E$  and  $\gamma$ , the average values of relevant ranges,  $E=55,000$  MPa and  $\gamma=26$  kN/m<sup>3</sup>, were adopted throughout the numerical enquiry.

The case study statue belongs to the art collection of the owners of the castle of Prampero, sited in Magnano in Riviera, province of Udine, which is one of the oldest and most famous examples of a medieval stronghold in the region of Friuli, Italy. The castle was severely damaged by an earthquake in 1976. After a long time of neglect, the first restoration intervention, concerning the northern tower, has been recently completed. A second restoration is expected soon, and it will concern the main wing of the castle, which partly collapsed after the earthquake, and for which a new destination as a museum has been suggested. According to the traditional exhibition settings in Italian museums, the statues will be accommodated on the ground floor. The renderings of the main façade and the longitudinal cross section of the building, which also incorporate the restored northern tower, are drawn in Figure 2. A total of eight marble and terracotta statues, with smaller or comparable dimensions to the case study one, will be placed on the ground floor, which covers the basement of the building. Stationary mount solutions were excluded by the art consultants of the exhibition planning, since they are extraneous to the common practice for small to medium scale non-metallic sculptures in Italy, due to the intrusion and possible local damage caused by mechanical connectors to their small base section(s). Adhesive glueing was not considered either, as it would be difficult to separate the sculptures from their pedestal or the floor in case of future changes in exhibition layouts.

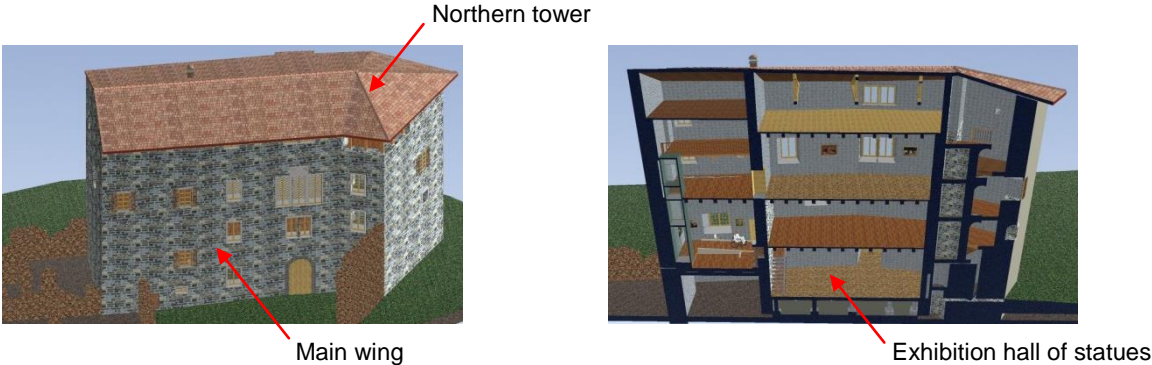


Figure 2. Renderings of the main wing and the northern tower of the castle of Prampero

The ground floor design plan is illustrated by the drawing in Figure 3, where the position of the case study statue in the exhibition set is highlighted with a square.

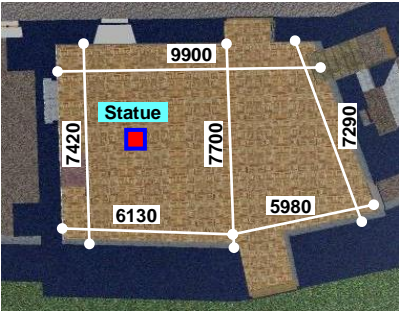


Figure 3. Architectural plan of the ground floor (dimensions in millimeters) and position of the case study statue

The plan is shaped as an irregular pentagon, with a surface area of about 85 m<sup>2</sup>. The floor is made of 55 mm-high HI-bond corrugated steel sheets, with a 55 mm-thick on-site cast reinforced concrete (R/C) slab on top. The main structure consists of primary and secondary beams in HEB 180 and HEB 100 Italian profiles, respectively, made of S235JR grade steel. Each primary beam spans over the shorter (transversal) dimension in plan, ranging from about 7.3 m to about 7.7 m, as shown in Figure 3, and is supported approximately at its midspan by a R/C column built on the basement level. This allows strongly reducing the bending moment, shear and vertical displacements induced by gravitational loads, and thus the cross section of the beams. This solution is mutually adopted for the fixed-base and base-isolated layouts of the floor. In the former case, each beam is joined to the

relevant midspan column by a horizontal steel plate bolted to the column top section, and is borne at both ends by the perimeter masonry walls of the hall. In base-isolated configuration, two other rows of R/C columns are built, for a total of 15 columns, to support 15 DFP sliders to be placed below the five main beams. These additional ten columns represent the only difference between the two design hypotheses for the floor. Renderings of the construction steps of the floor steel structure for the base-isolated solution, before casting the R/C slab, are illustrated in Figure 4.

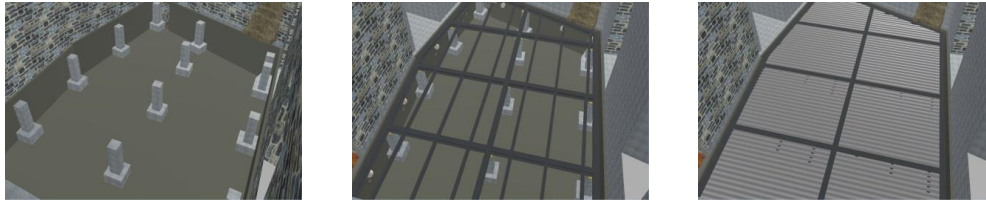


Figure 4 Construction steps of the ground floor steel structure in base-isolated configuration, before the casting of the R/C slab

The finite element model of the statue was generated by the ANSYS calculus program (Swanson Analysis Systems 2012), widely used in research studies dedicated to structural systems made of small tensile strength materials. The model consists of a full mesh of about 15,800 solid octahedral isotropic elements, reproducing the real geometry with reasonable accuracy (image on the right in Figure 1, where the reference coordinate system of the model is displayed too). A smeared-crack “concrete”-type constitutive model was assigned to each isotropic element. In this model, the Willam-Warnke triaxial failure domain (Willam and Warnke 1974) is adopted to simulate the ultimate compressive, tensile and mixed compressive–tensile triaxial ultimate response of the material. The classical Drucker-Prager yield criterion (Drucker and Prager 1952) is assumed by the program to reproduce plastic deformations. The main mechanical parameters of the “concrete”-type model are as follows:  $st_o$ =shear transfer coefficient for open crack;  $st_c$ =shear transfer coefficient for closed crack;  $f_{crus}$ =uniaxial crushing design stress, coinciding with compressive strength  $f_c$ ;  $f_{crus,b}$ =biaxial crushing stress;  $f_{crak}$ =uniaxial cracking stress, coinciding with tensile strength  $f_t$ ;  $E$ =Young modulus; and  $\nu$ =Poisson ratio. The parameters defining the surface of Drucker-Prager domain are:  $c$ =cohesion;  $\phi$ =friction angle; and  $\psi$ =dilatancy angle. The following basic values were adopted in the analysis:  $st_o=0.15$ , and  $st_c=0.8$ , which are typical choices for fine-grained materials, like the greyish Carrara marble constituting the case study sculpture;  $f_{crus}=40$  MPa,  $f_{crus,b}=1.2 \cdot f_{crus}=48$  MPa,  $f_t=1.5$  MPa,  $E=55,000$  MPa and  $\nu=0.2$ , according to the characteristics of the material illustrated above; and  $c=2.12$  MPa,  $\phi=30^\circ$  and  $\psi=0^\circ$  (associated flow rule), from literature suggestions concerning the plasticity domain for concrete and stone-type elements (Chen 1982).

A modal analysis of the statue was preliminarily carried out by assigning elastic properties to all the elements of the mesh. The first two vibration modes are mixed translational along  $y$ –rotational around  $z$  (first mode) and translational along  $x$ –rotational around  $z$  (second mode), with periods of 0.29 s and 0.26 s, respectively. The effective modal masses are equal to 55.9% of the total seismic mass along  $y$  and 23.4% around  $z$ , for the first mode, and 46.3% along  $x$  and 17.5% around  $z$ , for the second. Twelve modes are needed to activate summed modal masses greater than 90% along all three axes.

Rocking was simulated by a set of vertical “gap” (no-tension) interface elements, linking the perimeter joints of the base section of the pedestal to a corresponding set of joints belonging to the mesh of shell elements generated to schematise the upper R/C slab of the floor structure. The model of the latter was completed by a mesh of frame elements reproducing the primary and secondary steel beams. Sliding was simulated by horizontal elastic springs linking the same joints as the gap elements. Input ground motions were applied in the center of gravity of the floor, both in fixed-base and base-isolated layouts. The floor responded like a rigid diaphragm to each earthquake level.

## PERFORMANCE ASSESSMENT IN FIXED-BASE FLOOR DESIGN HYPOTHESIS

Seismic performance was investigated via incremental dynamic analysis (IDA), i.e. by progressively increasing the amplitude of the ground motion histories adopted as inputs, and by relating output data

to the reference performance levels formulated in section 2. The input accelerograms were generated in families of seven — which is the minimum number fixed by the Italian Standards to offer statistical significance to the results of a dynamic analysis, and to elaborate them in mean terms — both for the horizontal and vertical components of seismic action, from the pseudo-acceleration response spectra prescribed by the Italian seismic Standards (Italian Council of Public Works 2008) for the municipality of Magnano in Riviera. As required by the same Standards, as well as by Eurocode 8 (2004) and several other international seismic regulations, in each time-history analysis the accelerograms were applied in groups of three simultaneous components, i.e. two horizontal components parallel to  $x$  and  $y$ , respectively, with the first one selected from the first generated family of seven motions, and the second one selected from the second family, plus the vertical component. The application of the latter, not mandatory in the analysis of standard building structures, is strongly suggested for horizontal or nearly horizontal long-span members spanning 20 m or more, cantilever components longer than 5 m, beams supporting columns, pre-stressed components and base-isolated structures, as well as for any type of uplift-sensitive members, art objects and contents with free contact mounts included (Italian Council of Public Works 2008, Eurocode 8 2004). The role of the vertical component in time-history computations has been emphasized further in recent studies concerning rocking-prone assets (Papaloizou and Komodromos 2012) and base-isolated structures (Mazza et al 2012).

The generation of the families of accelerograms was carried out for several sets of horizontal and vertical spectra, built by varying the probability of exceedance ( $P_{VR}$ ) of the seismic action over the reference time period  $V_R$ . The latter was fixed at 150 years for castle of Prampero, obtained by multiplying the nominal structural life  $V_N$  of the building, equal to 100 years, by a coefficient of use  $c_u$  equal to 1.5, referred to its new destination as a museum.  $P_{VR}$  was varied by starting from a value of 95% and progressively decreasing it by 2% (i.e. the sequence of reference probabilities was: 95%, 93%, 91%, etc). This way, the spectral composition of input ground motions was preserved for each hazard level, unlike the traditional approach adopted in IDA enquiries (Vamvatsikos and Cornell 2002). Indeed in this approach, a single family of accelerograms generated from the response spectrum referred to a specific probability of exceedance, or a suite of real records selected from a ground motion database, are assumed as inputs; afterwards, they are kept unchanged throughout the analysis, by simply varying the amplitudes of the acceleration time-histories by means of a multiplicative scale factor.

A visual representation of the normative response spectra at 5% linear viscous damping ratio  $\xi$  for Magnano in Riviera is offered in Figure 5, showing the graphs relevant to the horizontal and vertical components for the four seismic hazard design levels established by the Italian Standards, i.e. Frequent Design Earthquake (FDE, with  $P_{VR}=81\%$ ); Serviceability Design Earthquake (SDE, with  $P_{VR}=63\%$ ); Basic Design Earthquake (BDE, with  $P_{VR}=10\%$ ); and Maximum Considered Earthquake (MCE, with  $P_{VR}=5\%$ ). By referring to topographic category (TC) equal to T1 — flat surface — and C-type soil — deep deposits of dense or medium-dense sand, gravel or stiff clay from several ten to several hundred meters thick — for the site of the castle, the peak ground acceleration (PGA) values for the four seismic levels are as follows: 0.183 g (FDE), 0.229 g (SDE), 0.448 g (BDE), and 0.491 g (MCE), for the horizontal component; and 0.058 g (FDE), 0.083 g (SDE), 0.339 g (BDE), and 0.465 g (MCE), for the vertical component, with  $g$ =acceleration of gravity.

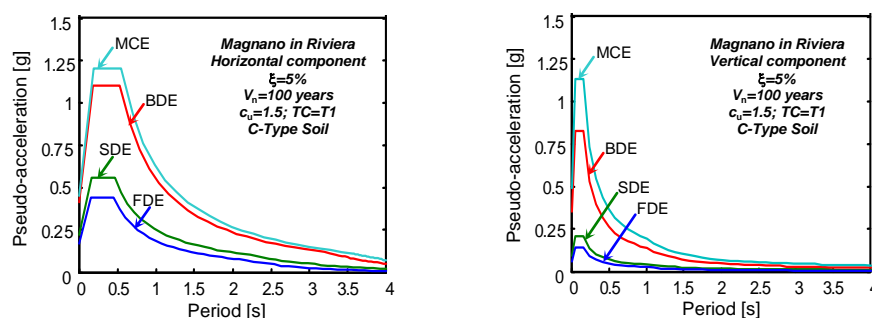


Figure 5. Normative pseudo-acceleration elastic response spectra for the horizontal and vertical components – Magnano in Riviera – FDE, SDE, BDE and MCE levels,  $\xi=5\%$ ,  $V_n=100$  years,  $c_u=1.5$ , TC=T1, and C-type soil

The results of the performance assessment enquiry are recapitulated in Table 1, where the PGAs of the two horizontal components and the associated vertical component of the input seismic action causing the attainment of the limit conditions for the four performance levels are recapitulated, along with corresponding  $P_{VR}$  values. Concerning No rocking and Damage control PLs, the evaluation of relevant limit conditions was carried out by referring to the criteria presented in section 2, i.e. the localization of at least five uplifts with amplitude no lower than 0.5 mm, for the former, and a crack spread in at least 5% of Gauss points of the smeared-crack model, for the latter.

Table 1. Summary of the performance assessment analysis of the statue in fixed-base floor design hypothesis

Performance levels	Attainment of Limit Conditions		
	PGA – Horizontal components (g)	PGA – Vertical component (g)	$P_{VR}$ (%)
Rest	0.114	0.020	95
No rocking	0.157	0.043	89
Damage control/Artistic value safety	0.191	0.061	79
Collapse prevention	0.228	0.083	63

The data in Table 1 highlight that the limit conditions of the four PLs are exceeded for PGA values below (Rest and No rocking) or just beyond (Damage control/Artistic value safety) FDE ones, and virtually coinciding (Collapse prevention) with SDE ones. These correlations point to poor seismic performance of the statue, for the basic set of mechanical parameter values adopted in the smeared-crack finite element analysis.

As observed in the previous section, the uniaxial tensile strength  $f_t$  was varied in the numerical enquiry from the basic choice of 1.5 MPa through 3 MPa. For the latter value, the limit conditions for Damage control/Artistic value safety and Collapse prevention levels were reached for the following PGAs of the horizontal and vertical components: 0.203 g–0.066 g ( $P_{VR}=75\%$ ), and 0.251 g–0.097 g ( $P_{VR}=57\%$ ), respectively. The differences with the values obtained for  $f_t=1.5$  MPa are small, revealing a limited influence of tensile strength, for the considered  $f_t$  range of technical interest, on the two performance levels involving the activation of cracks (for Rest and No rocking PLs the response was totally uncracked).

The effects of sliding were negligible up to the attainment of numerical collapse, as highlighted by the very low peak horizontal base displacements recorded at the final step of IDA, equal to about 0.3 mm. This was confirmed by a supplementary enquiry developed by removing the horizontal springs placed at the base of the model, which produced no appreciable alterations to the data in Table 1. Therefore, the case study sculpture resulted to be sensitive only to rocking and related uplift effects.

As way of example of the responses obtained at the limit conditions of the four PLs, the following drawings and graphs are reproduced in Figures 6 through 9, for the most demanding among the seven groups of accelerograms used in the analysis: for Rest and No rocking, the normal stress distribution in the model, with the two areas subjected to the highest tensile stresses, that is, the left leg knee and the rear portion of the neck, highlighted by red ellipses (Figure 6); the cracked configuration of the same two critical zones, plotted in zoomed view and coloured in light grey, for Damage control/Artistic value safety (Figure 7); the ultimate cracked configuration of the front and rear portions of the neck, again in zoomed view, for Collapse prevention (Figure 8); and the vertical displacement time-histories of the joint situated on the rear left corner of the pedestal, for No rocking and Collapse prevention (Figure 9).

The peak tensile stress values in the plots of Figure 6 are equal to about 0.8 MPa (Rest) and 1.2 MPa (No rocking), both lower than  $f_t$ . These values quantitatively confirm the uncracked response for these two PLs. The mean values obtained from the response to the seven groups of accelerograms are only slightly lower (about 0.76 MPa and 1.14 MPa, respectively), highlighting the limited scattering of response for the suites of artificial ground motions used as input in the analysis. The plots in Figure 7 outline a noticeable set of cracks that would be clearly visible in the real statue, both in the leg and the neck, also figuratively showing the attainment of Damage control/Artistic value safety PL. The activation of cracks is recorded in 5.6% of Gauss points of the model, for the most demanding group

of accelerograms, and 5.1% in mean terms over the seven groups, i.e. only just above the 5% threshold assumed as limit conditions for this PL.

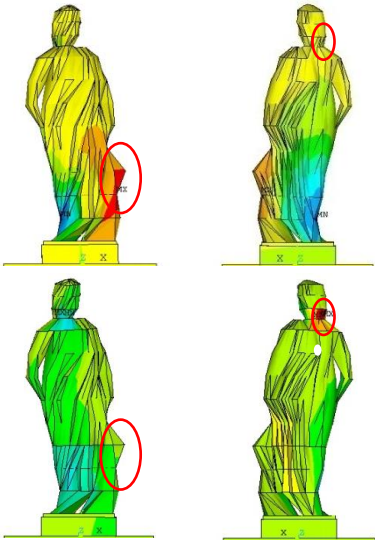


Figure 6. Normal stress distributions for the limit conditions of Rest (upper two images) and No rocking obtained from the most demanding among the seven groups of accelerograms

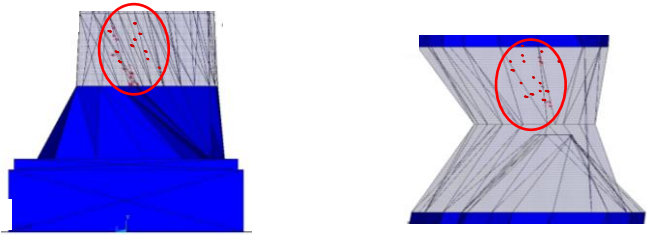


Figure 7. Cracked configurations of the left leg knee (left image) and the rear portion of the neck for the limit conditions of Damage control/Artistic value safety obtained from the most demanding among the seven groups of accelerograms

The cracked configuration depicted in Figure 8 clearly illustrates that numerical collapse, and thus the achievement of the limit condition for Collapse prevention PL, is caused by the local failure of the base section of the neck, which is the most vulnerable area of the model.

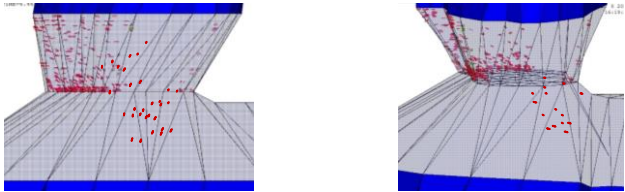


Figure 8. Cracked configurations of the front (left image) and rear portion of the neck for the limit conditions of Collapse prevention obtained from the most demanding among the seven groups of accelerograms

The vertical displacement time-history corresponding to the achievement of the limit conditions for No rocking, plotted in the left graph of Figure 9, shows six peaks greater than the assumed threshold of 0.5 mm (highlighted by a red horizontal segment in the graph), with a maximum of 1.3 mm. Each of the remaining six groups of input motions produced five peaks greater than 0.5 mm, giving rise to a mean maximum peak of 1.1 mm over the seven groups. As illustrated in the right graph of Figure 9, the time-history relevant to the limit conditions of Collapse prevention stopped immediately after the attainment of the maximum uplift, equal to 6.6 mm, as a consequence of the

divergence of the numerical solution at the subsequent step. Similar results are observed for the remaining six groups of accelerograms.

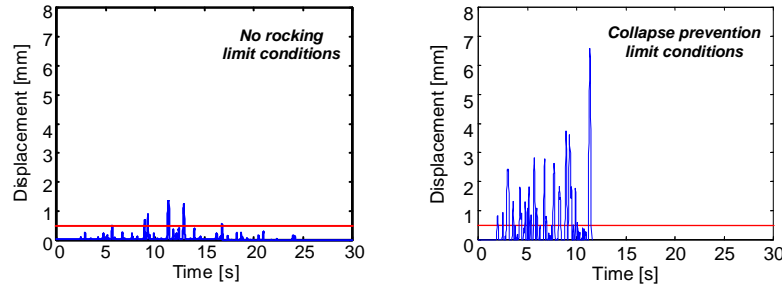


Figure 9. Vertical displacement time-histories of the joint situated on the rear left corner of the pedestal for the limit conditions of No rocking and Collapse prevention obtained from the most demanding among the seven groups of accelerograms

A final observation concerns the performance objectives pursued in the rehabilitation and partial rebuilding design of Prampero castle, which are as follows: Operational level for FDE; Immediate Occupancy for SDE; and Life Safety for BDE and MCE, with the three PLs defined as in (ASCE 2006). Based on these design assumptions, the case study sculpture would collapse at the same SDE level for which Immediate Occupancy guarantees, instead, a totally undamaged structural response of the building, and at most very limited and easily repairable non-structural damage, essentially limited to plasters. This much higher vulnerability of an important artistic content represents a noticeable drawback in the global seismic response of the monumental building, prompting the implementation of the base-isolation protective solution discussed in the next section.

## BASE-ISOLATED FLOOR DESIGN HYPOTHESIS

As shown in the drawing in Figure 10, the double-friction pendulum sliders (Fenz and Constantinou 2006, Christopoulos and Filiatrault 2006) selected as isolating devices for this design hypothesis consist of two facing spherical concave surfaces, separated by an articulated double friction slider, which produce two independent pendulum response mechanisms. The DFP devices in standard production are characterized by identical properties of the two surfaces, and namely, by referring to the nomenclature in Figure 10: radius  $R$ ; slider center-to-surface distance  $h$  (i.e. the distance between the “pivot point”  $P$  of the articulated slider and the face of each spherical surface); effective pendulum length  $R-h$  (i.e. the distance between  $P$  and the center  $C$  of each surface); diameter of the horizontal projection of the spherical surface  $D$ ; and friction coefficient  $\mu$ . The resulting effective pendulum length  $L_{DFP}$  of the isolator is equal to twice the effective pendulum length of each surface, i.e.  $L_{DFP} = 2 \cdot (R-h) = 2R-2h$ .

The equivalent vibration period of a DFP,  $T_e$ , and the equivalent viscous damping ratio,  $\xi_e$ , are expressed as:

$$T_e = 2\pi \sqrt{\frac{1}{g \left( \frac{1}{L_{DFP}} + \frac{\mu}{d_{max}} \right)}} \quad (1)$$

$$\xi_e = \frac{2}{\pi} \cdot \frac{1}{\frac{d_{max}}{\mu L_{DFP}} + 1} \quad (2)$$

where  $g$ =acceleration of gravity, and  $d_{max}$ =maximum displacement of the device along all directions in plan. Based on a preliminary sizing carried out by estimating the maximum displacement demand for the MCE seismic level, the following mechanical and geometrical properties were selected for the

isolators, as derived from the reference manufacturer’s catalogue (FIP 2013):  $L_{DFP}=3125$  mm;  $d_{max}=250$  mm;  $\mu=0.025$ ;  $D=490$  mm;  $T_e=3.1$  s; and  $\xi_e=15.2\%$ . The height  $H$  (Figure 10) is equal to 94 mm.

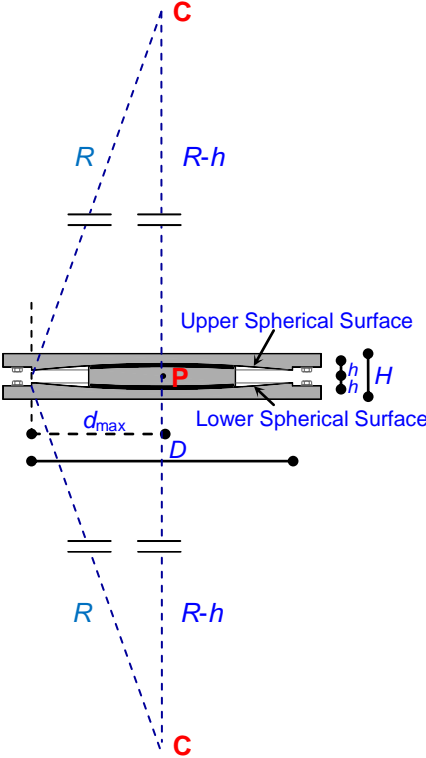


Figure 10. Cross section of a DFP isolator with equal sliding surfaces

A drawing illustrating the details of installation of an isolator placed on top of a lateral column is presented in Figure 11. The depth of the continuous carving of the perimeter walls of the hall, reinforced by a C-shaped steel beam composed of three welded plates, was dimensioned in order to accommodate  $d_{max}$ . The only equipment situated on the floor is the power installation. To safely accommodate  $d_{max}$  too, power cables are arranged in a circular winding prior to connecting them to the floor structure, according to a classical and inexpensive installation layout adopted for base-isolated buildings (Sorace and Terenzi 2001, 2008).

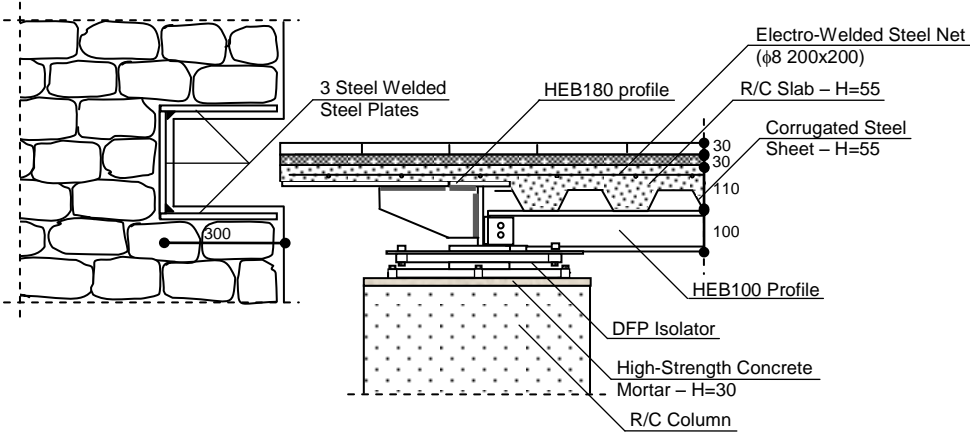


Figure 11. Installation details of a DFP isolator situated on top of a lateral column (dimensions in mm)

The results of the analysis show that the limit conditions of the Rest performance level, and consequently of the three highest PLs, are reached for a theoretical amplitude of seismic action greater than the one of MCE. The response to the latter is characterised by peak tensile stress values, surveyed again in the left leg knee and the rear portion of the neck, equal to about 0.5 MPa, i.e. only 1/3 of  $f_t$ .

The maximum horizontal displacements of the mobile floor for MCE are lower than  $d_{\max}$ , and namely equal to 223 and 211 mm along the longitudinal and transversal directions of the floor in plan, respectively, for the most demanding among the seven groups of accelerograms.

A supplementary control was carried out by developing a further set of time-history analyses with the most demanding real ground motions recorded in Gemona, a neighbor town to Magnano in Riviera, during the Friuli earthquake in 1976. These ground motions, characterized by a distance of 6.2 km from the surface projection of the causative fault, a fault-thrust mechanism, and moment magnitude  $M_w=5.9$ , are the E-W, N-S and up-down (vertical) components of the main shock recorded on September 15, with PGAs of 0.642 g, 0.329 g and 0.485 g, respectively, and the pseudo-acceleration elastic response spectra at 5% linear viscous damping ratio plotted in Figure 12. As observed in the Introduction, these ground motions caused very severe damage and partial disruption to the castle of Prampero, situated at about 1.5 km from Gemona recording station, which had been already partly damaged by a comparably demanding ground motion sequence occurred on May 6.

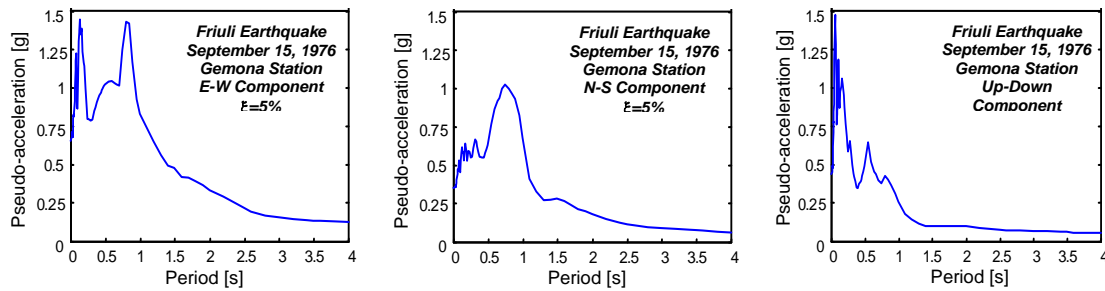


Figure 12. Pseudo-acceleration elastic response spectra at  $\xi=5\%$  of the E-W and N-S horizontal components, and the vertical component recorded in Gemona station on September 15, 1976

The application of the real motions produced a slightly lower response of the redesigned structure of the castle as compared to the normative MCE-scaled groups of artificial accelerograms. Indeed, the two spectral peaks of the E-W component, situated at about 0.8 s and 0.1 s, and the peaks of the N-S and up-down components, nearing 0.75 s and 0.1 s, respectively, are outside the range [0.3 s – 0.6 s] of the main vibration periods of the masonry structure of the castle. All remaining ordinates, up to about 2 s, are lower for the real motions.

On the other hand, the spectral ordinates of the latter are higher than the MCE ones in the period range [3 s–3.5 s], which includes the fundamental vibration period of the base-isolated floor. The results of the analysis in this configuration highlight peak displacements of 241 and 226 mm along the longitudinal and transversal directions in plan, that is, 8% and 7% greater than the values found for the most demanding MCE-scaled accelerograms, respectively, but still lower than the maximum available displacement  $d_{\max}$  of the isolators.

The cost of the fifteen DFP devices amounts to about 24,000 Euros, installation works included, plus the construction costs of the ten additional R/C columns required by the base-isolated solution, equal to about 15,000 Euros, for a rounded total of 39,000 Euros. This is about 20% lower than the total cost estimated for the independent base isolation of each one of the eight statues to be placed in the exhibition hall, averagely computed at 6000 Euros per statue, as deducted from several interventions carried out in the past few years, with various types of isolation systems, on small-to-medium sized sculptures.

## CONCLUSIONS

The seismic performance assessment enquiry carried out on a marble statue, representative of a wide stock of sculptures with similar characteristics, confirmed the high vulnerability of these artworks when they are installed with traditional mount techniques, as repeatedly surveyed in post-earthquake field inspections of museums and exhibition buildings.

The wider set of performance levels formulated and set up in this study, as compared to basic literature assessment analyses of art objects, and the explicit simulation of rocking in the time-history

investigation, allowed following more accurately the evolution of response in the statue, from the earliest decompression of a pedestal joint through numerical collapse.

The unconventional base-isolation solution proposed for the advanced protection of the case study statue, as well as of other seven sculptures to be placed on the ground floor of the new museum wing of the castle of Prampero, guarantees extreme enhancement of their seismic performance, at very small additional construction costs.

Furthermore, this solution causes no architectural intrusion or concern from an aesthetic viewpoint, since the statues are installed exactly like in traditional free contact mounts on non seismically isolated floors.

## ACKNOWLEDGEMENTS

The study reported in this paper was financed by the Italian Department of Civil Protection within the ReLUIS-DPC Project 2014/2016. The authors gratefully acknowledge this financial support.

## REFERENCES

- ASCE (2006) Seismic rehabilitation of existing buildings – ASCE/SEI 41-06, ASCE, Reston, VA.
- Augusti G and Ciampoli M (1996) “Guidelines for seismic protection of museum contents,” *Proceedings of 11<sup>th</sup> WCEE*, Acapulco, Mexico, Paper 1668, CD-ROM.
- Caliò I and Marletta M (2003) “Passive control of the seismic rocking response of art objects,” *Engineering Structures*, 25:1009-1018.
- Christopoulos C and Filiatrault A (2006) Principles of passive supplemental damping and seismic isolation, IUSS Press, Pavia, Italy.
- Chen WF (1982) Plasticity in reinforced concrete, Mc-Graw Hill, New York, NY.
- Drucker DC and Prager W (1952) “Soil mechanics and plastic analysis for limit design,” *Quarterly of Applied Mathematics*, 10:157-165.
- Eurocode 8 (2004) Design of structures for earthquake resistance. Part 1: General rules, seismic actions and rules for buildings, European Commission, Bruxelles, Belgium.
- Fenz DM and Constantinou MC (2006) “Behaviour of the double concave friction pendulum bearing,” *Earthquake Engineering and Structural Dynamics*, 35:1403-1424.
- FIP (2013) Anti-seismic devices product division, <http://www.fip-group.it>.
- Italian Council of Public Works (2008) Technical Standards on Constructions [in Italian], Rome, Italy.
- Mazza F, Vulcano A and Mazza M (2012) “Nonlinear dynamic response of RC buildings with different base-isolation systems subjected to horizontal and vertical components of near-fault ground motions,” *The Open Construction & Building Technology Journal*, 6:373-383.
- Papaloizou L and Komodromos P (2012) “The effect of earthquakes’ vertical components on ancient multi-drum structures,” *Proceedings of 15<sup>th</sup> WCEE*, Lisbon, Portugal, Paper 314, CD-ROM.
- Scesi L, Papini M and Gattinoni P (2006) Geologia applicata: il rilevamento geologico tecnico [in Italian], Editrice Ambrosiana, Milan, Italy.
- Sorace S (1996) “Creep in building stones under tensile conditions,” *Journal of Engineering Materials and Technology ASME*, 118:461-467.
- Sorace S (1998) “Time-delayed rupture of stones under low tensile and bending stress states,” *Materials and Structures*, 31:428-432.
- Sorace S and Terenzi G (2001) “Non-linear dynamic modelling and design procedure of FV spring-dampers for base isolation,” *Engineering Structures*, 23:1556-1567.
- Sorace S and Terenzi G (2008) “Analysis and demonstrative application of a base isolation/supplemental damping technology,” *Earthquake Spectra*, 24:775-793.
- Swanson Analysis System (2012) ANSYS, Engineering Analysis System – Theory/Users’ manual, Canonsburg, PA.
- Vamvatsikos D and Cornell CA (2002) “Incremental dynamic analysis,” *Earthquake Engineering and Structural Dynamics*, 31:491-534.
- Willam KJ and Warnke EP (1974) “Constitutive model for the triaxial behaviour of concrete,” *Proceedings of IABSE Seminar on Concrete structures subjected to triaxial stresses*, Bergamo, Italy, 1-30.